Journal of Pathology
J Pathol September 2021; **255:** 72–83
Published online 28 July 2021 in Wiley Online Library (wileyonlinelibrary.com) DOI: 10.1002/path.5739

ORIGINAL PAPER

AZD8055 enhances *in vivo* efficacy of afatinib in chordomas

Tianna Zhao[1], I-Mei Siu[1], Tara Williamson[1], Haoyu Zhang[1], Chenchen Ji[1], Peter C Burger[2], Nick Connis[3], Jacob Ruzevick[1], Menghang Xia[4], Lucia Cottone[5], Adrienne M Flanagan[5,6], Christine L Hann[3] and Gary L Gallia[1,3,7]*

[1] *Department of Neurosurgery, Johns Hopkins University School of Medicine, Baltimore, MD, USA*
[2] *Department of Pathology, Johns Hopkins University School of Medicine, Baltimore, MD, USA*
[3] *Department of Oncology, Johns Hopkins University School of Medicine, Baltimore, MD, USA*
[4] *National Center for Advancing Translational Sciences, National Institutes of Health, Bethesda, MD, USA*
[5] *Department of Pathology, UCL Cancer Institute, University College London, London, UK*
[6] *Histopathology Department, Royal National Orthopaedic Hospital, Stanmore, UK*
[7] *Department of Otolaryngology/Head and Neck Surgery, Johns Hopkins University School of Medicine, Baltimore, MD, USA*

**Correspondence to: GL Gallia, Department of Neurosurgery, Johns Hopkins University School of Medicine, Cancer Research Building II, Baltimore, MD 21231, USA. E-mail: ggallia1@jhmi.edu*

Abstract

Chordomas are primary bone tumors that arise in the cranial base, mobile spine, and sacrococcygeal region, affecting patients of all ages. Currently, there are no approved agents for chordoma patients. Here, we evaluated the anti-tumor efficacy of small molecule inhibitors that target oncogenic pathways in chordoma, as single agents and in combination, to identify novel therapeutic approaches with the greatest translational potential. A panel of small molecule compounds was screened *in vivo* against patient-derived xenograft (PDX) models of chordoma, and potentially synergistic combinations were further evaluated using chordoma cell lines and xenograft models. Among the tested agents, inhibitors of EGFR (BIBX 1382, erlotinib, and afatinib), c-MET (crizotinib), and mTOR (AZD8055) significantly inhibited tumor growth *in vivo* but did not induce tumor regression. Co-inhibition of EGFR and c-MET using erlotinib and crizotinib synergistically reduced cell viability in chordoma cell lines but did not result in enhanced *in vivo* activity. Co-inhibition of EGFR and mTOR pathways using afatinib and AZD8055 synergistically reduced cell viability in chordoma cell lines. Importantly, this dual inhibition completely suppressed tumor growth *in vivo*, showing improved tumor control. Together, these data demonstrate that individual inhibitors of EGFR, c-MET, and mTOR pathways suppress chordoma growth both *in vitro* and *in vivo*. mTOR inhibition increased the efficacy of EGFR inhibition on chordoma growth in several preclinical models. The insights gained from our study potentially provide a novel combination therapeutic strategy for patients with chordoma.

Keywords: chordomas; small molecule inhibitors; preclinical models; EGFR; mTOR

Received 11 September 2020; Revised 17 May 2021; Accepted 9 June 2021

Conflict of interest statement: AMF is currently President of The Pathological Society, which owns this journal. CLH has served in a consultant/advisory role for AbbVie, AstraZeneca, BMS, Genentech/Roche, and GSK, and has received research funding (directly to the institution) from AbbVie, Amgen, AstraZeneca, BMS, GSK, and Merrimack during the conduct of this study. The other authors declare no potential conflicts of interest.

Introduction

Chordomas are rare, locally aggressive bone tumors that arise in the cranial base, mobile spine, and sacrum. These malignant tumors occur in all age groups with a median age at diagnosis of approximately 58 years [1] and are characterized by the expression of brachyury, which plays an essential role in chordoma development [2–4]. Surgical resection often with adjuvant radiotherapy is considered as standard treatment in chordoma and provides the best chance for long-term control [5]. However, the tumor recurs frequently and metastases have been reported to occur in up to 40% of cases [6]. Median survival for patients is 7–9 years [1,7]. The proximity of chordomas to vital neurovascular structures often limits the complete removal of tumor and also reduces the efficacy of radiotherapy; thus, there is an unmet need for the development of adjuvant therapies. Currently, there are no FDA-approved therapeutic agents available for patients with chordoma and conventional cytotoxic chemotherapy is largely ineffective in chordoma treatment [6].

Over the past decade, there have been increasing efforts to better understand chordoma biology and develop novel therapeutic strategies. We established and characterized the first reported chordoma patient-derived xenograft

(PDX) [8]. Consistent with clinical observations [9–12], epidermal growth factor receptor (EGFR) signaling was activated in this PDX. Erlotinib, an inhibitor of EGFR, significantly but incompletely suppressed chordoma growth *in vivo* [13], suggesting that inhibition of other growth-promoting pathways may be required for increased efficacy.

In the current work, we evaluated the anti-tumor activity of a panel of agents alone and in combination in a variety of chordoma models. More specifically, using our initial PDX model, we tested agents identified in a high-throughput screen in the NIH Chemical Genomics Center (NCGC, now part of the National Center for Advancing Translational Sciences, NCATS) which exhibited *in vitro* efficacy against chordoma cell lines [14] and inhibitors of pathways known to be expressed in chordoma or shown to have benefit in a phase 2 clinical trial [15–18]. We further evaluated the anti-tumor activity of compounds with significant *in vivo* efficacy in a novel chordoma PDX model established and reported here. Subsequently, we evaluated the enhanced efficacy of combination therapy by co-targeting EGFR and c-MET or co-targeting EGFR and mTOR signalings using chordoma cell lines and PDX models.

Materials and methods

Ethics approval/patient consent statement

Ethical approval was obtained from the UK Cambridgeshire 2 Research Ethics Service (reference 09/H0308/165) for the generation of the chordoma PDX model in the UK and transportation to the USA. All animal experiments performed in the USA were approved by the Johns Hopkins University Animal Care and Use Committee (protocols: MO20M90 and MO17M96).

Compounds and reagents

Erlotinib, crizotinib, afatinib, vandetanib, and AZD8055 were obtained from LC Laboratories (Woburn, MA, USA), and BIBX 1382 was obtained from Tocris Bioscience (Bristol, UK). All other compounds were kindly provided by the NCGC. Compounds used in this study are detailed in Table 1. Toxicity studies were performed to determine the maximal tolerated dose for *in vivo* studies. For *in vitro* studies, all compounds were dissolved in dimethyl sulfoxide (DMSO; MilliporeSigma, Burlington, MA, USA), and DMSO was used as a vehicle control. For *in vivo* studies, BIBX 1382, vandetanib, idarubicin, SAHA, staurosporine, and 17-AAG were dissolved in 10% DMSO, whereas crizotinib, imatinib, erlotinib, afatinib, and AZD8055 were dissolved in 1X PBS. Either DMSO or PBS (Thermo Fisher Scientific, Waltham, MA, USA) was used as a vehicle control.

Animals and PDX models

JHH-2009-011, a primary human chordoma xenograft model, has been described previously [8]. For generation of the UCL/JHH chordoma PDX, the tumor sample was collected as part of the University College London (UCL)/H Biobank for Health and Disease that is covered by the Human Tissue Authority license 12 055: project EC17.1. The PDX was established in SCID mice in AMF's laboratory at UCL. Tumor-bearing mice were shipped to Johns Hopkins and tumors subcloned into athymic nude mice (Charles River Laboratories, Wilmington, MA, USA), generating the UCL/JHH PDX.

For *in vivo* animal studies, fresh tumor was harvested, minced into 1 mm^3 pieces with razor blades, mixed 1:1 with phenol red-free Matrigel (BD Biosciences, San José, CA, USA), and injected subcutaneously into the rear flanks of 4- to 6-week-old athymic nude mice. Mice were randomly grouped to receive drug treatment when tumors achieved an average volume between 200 and 250 mm^3. Animal weights were measured every 7 days and tumor volume was assessed by caliper and calculated using the formula tumor volume (mm^3) $= \pi/6 \times$ length (mm) $\times$ width (mm) $\times$ height (mm). Mice were euthanized if the tumor volume reached a limit of 2000 mm^3. Tumor growth inhibition was defined as [1 – (mean volume of treated tumors)/(mean

Table 1. Target, route of administration, and dosage of compounds.

Compound	Inhibition target	Administration	Dose
BIBX 1382	EGFR	Oral gavage	20 mg/kg, 5 days per week
Vandetanib	EGFR, RET, VEGFR	Oral gavage	50 mg/kg per day [19]
Crizotinib	MET, ALK	Oral gavage	25 mg/kg, 5 days per week [20]
Idarubicin	Topoisomerase II	IP injection	0.156 mg/kg, 2 days per week
SAHA	Histone deacetylase	IP injection	100 mg/kg, 2 days per week [21]
Staurosporine	Protein kinases	IP injection	1.5 mg/kg for 5 days [22]
17-AAG	Heat shock protein 90	IP injection	25 mg/kg, 5 days per week [23]
Imatinib	PDGFR	Oral gavage	100 mg/kg per day [24]
Erlotinib	EGFR	Oral gavage	50 mg/kg, 5 days per week [13]
Afatinib	EGFR, HER2	Oral gavage	20 mg/kg, 5 days per week [25]
AZD8055	mTOR	Oral gavage	10 mg/kg, 5 days per week [26]

17-AAG, 17-allylamino geldanamycin; ALK, anaplastic lymphoma kinase; EGFR, epidermal growth factor receptor; HER2, human epidermal growth factor receptor 2; IP, intraperitoneal; MET, mesenchymal epithelial transition factor receptor; mTOR, mammalian target of rapamycin; PDGFR, platelet-derived growth factor receptor; RET, rearranged during transfection; SAHA, suberoylanilide hydroxamic acid; VEGFR, vascular endothelial growth factor receptor.

volume of control tumors)] × 100% [27] and calculated at the day of harvest.

Short tandem repeat analysis

Short tandem repeat (STR) analysis of the JHH/UCL PDX and the parental tumor was conducted using the PowerPlex 16 HS Kit (Promega, Madison, WI, USA) that analyses differences at 16 distinct hypervariable genetic loci by the Public Health England Culture Collections (Salisbury, UK). STR analysis of the four chordoma cell lines U-CH1, U-CH2, JHC7, and UM-Chor1 used in this study was performed using the GenePrint 10 System (Promega), analyzed using GeneMapper v4.0 software (Thermo Fisher Scientific), and compared with the reference profile found in the ATCC database (ATCC, Manassas, VA, USA; https://www.atcc.org/en/search-str-database). Sample authenticity was assessed following 80% match criteria according to ATCC standards (ANSI/ATCC ASN-0002: Authentication of Human Cell Lines: Standardization of STR Profiling).

Histology and immunohistochemistry

Fresh xenograft tissues were fixed in 10% buffered formalin solution (Thermo Fisher Scientific), dehydrated, embedded in paraffin, and serially sectioned at 5 μm. For histology, slides were stained with hematoxylin and eosin (H&E). For immunohistochemistry analysis, rehydrated slides were placed in 1X citrate buffer (BioGenex, Fremont, CA, USA) and heated for antigen retrieval at 95 °C for 20 min. The sections were incubated with primary antibodies overnight followed by incubation with MultiLink + HRP label detection systems (BioGenex). All antibodies and antibody dilutions used for immunohistochemistry are listed in supplementary material, Table S1.

Receptor tyrosine kinase (RTK) array

The expression of human phosphorylated RTK was detected by a proteome profiler array kit (ARY001B; R&D Systems, Minneapolis, MN, USA), and 1 mg of protein extracted from xenograft tissue was loaded for RTK array analysis according to the protocol described in the datasheet.

Cell lines and culture conditions

Four human chordoma cell lines (U-CH1, U-CH2, JHC7, and UM-Chor1) were used in this study. U-CH1 and U-CH2 cells were obtained from the Chordoma Foundation. JHC7 cells [28] were kindly provided by Alfredo Quiñones-Hinojosa and UM-Chor1 cells were purchased from the ATCC. All cell lines were authenticated by STR analysis (supplementary material, Table S2). U-CH1, U-CH2, and UM-Chor1 cells were grown in 0.1% gelatin (MilliporeSigma)-coated culture flasks containing chordoma medium of Iscove's Modified Dulbecco's Medium (IMDM; Thermo Fisher Scientific) and RPMI 1640 (Thermo Fisher Scientific) mixed at 4:1 as described previously [13]. JHC7 cells were cultured in MesenPRO RS Medium (Thermo Fisher Scientific). All cells were maintained in a humidified atmosphere of 5% CO_2 at 37 °C.

Cell viability and cytotoxicity assay

Chordoma cells were plated at a density of 2000 cells per well in 96-well plates and cultured for 24 h before exposure to compounds and vehicle control. After 48 h incubation, cell viability was measured either using a CellTiter-Glo® Luminescent Cell Viability Assay (Promega) on a VICTOR 3 1420 Multilabel Counter (PerkinElmer, Waltham, MA, USA) or by trypan blue assay (MilliporeSigma). Cell viability was presented as the percentage of surviving cells in drug-treated cells relative to DMSO-treated control cells. Cytotoxicity was determined with a CyQUANT™ lactate dehydrogenase (LDH) Cytotoxicity Assay Kit (Thermo Fisher Scientific), and the percentage of cytotoxicity was calculated according to the manufacturer's instructions. Data were plotted using GraphPad Prism version 6 (GraphPad Software, San Diego, CA, USA).

Colony formation assay

U-CH1, U-CH2, and UM-Chor1 cells were seeded in six-well plates at a density of 500 cells per well. Seven days after plating, cells were treated with vehicle (DMSO), 0.5 μM afatinib alone, 5 μM AZD8055 alone, and in combination. After 72 h incubation, medium was removed and replaced with fresh medium without drug for 14–21 days. For colony staining, cells were first fixed with 4% paraformaldehyde for 20 min and then stained with 0.5% crystal violet. Colonies were assessed visually, and colonies containing greater than 50 cells were counted.

Combination therapy synergy quantitation

Cells were treated for 48 h with combinations of a series of concentrations of erlotinib (1.25, 2.5, 5, 10, 20 μM) and crizotinib (1, 2, 4, 8, 16 μM) or afatinib (0.25, 0.5, 1, 2, 4, 8 μM) and AZD8055 (0.3125, 0.625, 1.25, 2.5, 5, 10 μM). Cell viability was examined using a CellTiter-Glo® Luminescent Cell Viability Assay (Promega). The synergy of drug combinations was evaluated using the Chou–Talalay method [29]. Multiple drug dose-effects were calculated by CompuSyn software to determine the combination index (CI), a quantitative definition for additive effect ($CI = 1$), synergism ($CI < 1$), and antagonism ($CI > 1$) of drug combinations.

Protein extraction and western blot analyses

Cells were harvested after 24–48 h of drug treatments; xenograft tissues were collected at 49 days with co-treatment of erlotinib and crizotinib or at 56 days following co-treatment of afatinib with AZD8055. Cells and tissues were lysed in RIPA lysis buffer (MilliporeSigma)

containing fresh protease and phosphatase inhibitor cocktail (Thermo Fisher Scientific). Xenograft tissue was disrupted by bead-beating for 30 s twice with a 2-min interval on ice. All tissue lysates were centrifuged at 13 000 rpm × 10 min at 4 °C. Proteins were separated on 4–12% Bis-Tris Gels (Thermo Fisher Scientific) and transferred onto polyvinyl difluoride membranes (MilliporeSigma). Antibodies and antibody dilutions used for western blot are described in supplementary material, Table S1. Protein bands were visualized using the Odyssey™ Infrared Imager (LI-COR Biosciences, Lincoln, NE, USA) according to the manufacturer's instructions. Original images of western blots are shown in supplementary material, Appendix S1.

Statistics

All quantitative data are presented as mean ± standard error of the mean (SEM). Tumor growth curves were plotted, and the statistical significance of differences was determined by independent sample two-tailed *t*-tests or two-way ANOVA followed by Tukey's multiple comparisons (GraphPad Software). $p < 0.05$ was considered statistically significant.

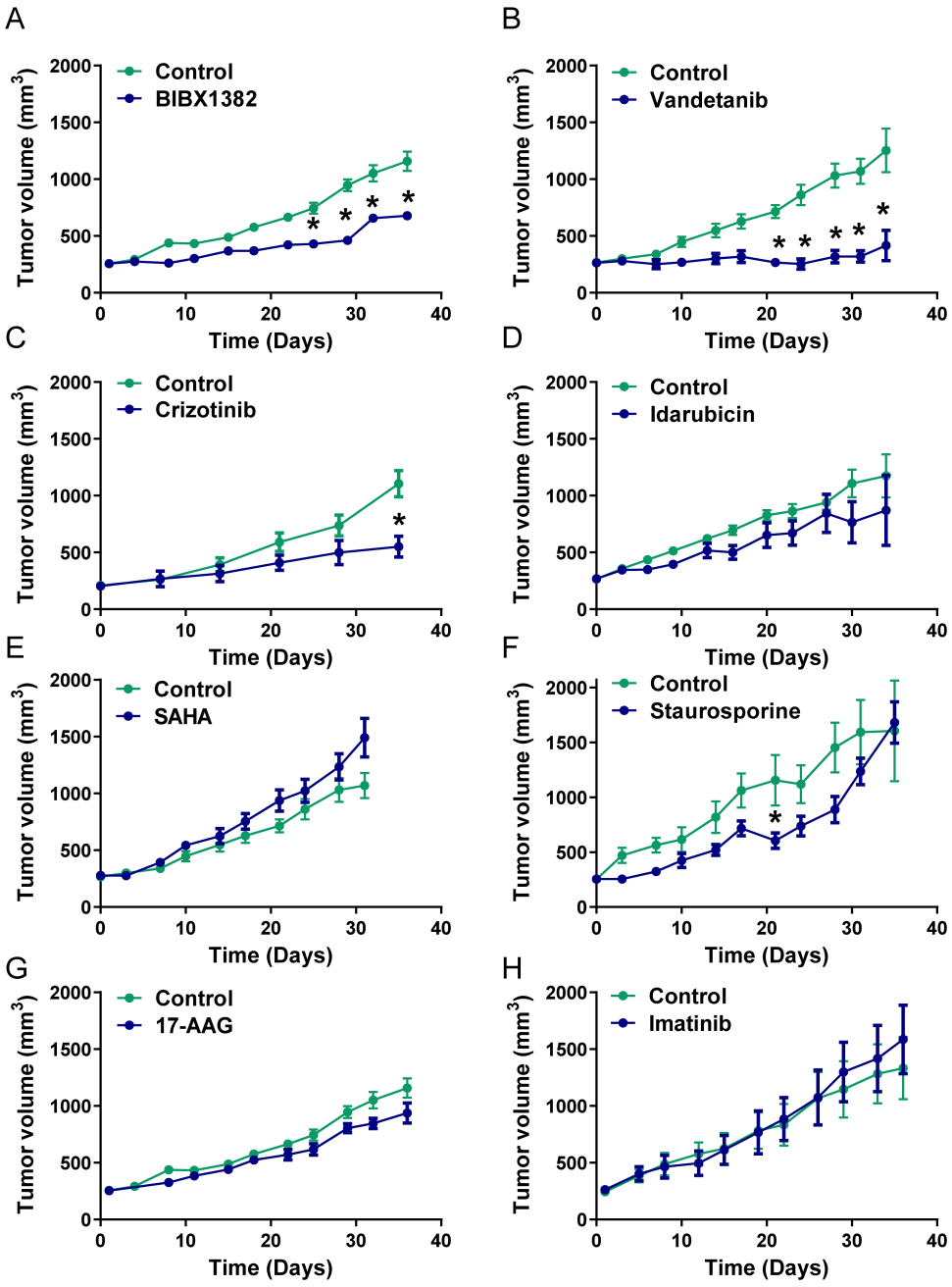

Figure 1. BIBX 1382, vandetanib, and crizotinib suppress chordoma growth in PDX JHH-2009-011. Tumor growth of PDX JHH-2009-011 in athymic nude mice treated with BIBX 1382 (A, $n = 9$), vandetanib (B, $n = 7$), crizotinib (C, $n = 5$), idarubicin (D, $n = 10$), SAHA (E, $n = 8$), staurosporine (F, $n = 8$), 17-AAG (G, $n = 9$), and imatinib (H, $n = 7$) is shown. Single treatments of BIBX 1382 and 17-AAG or vandetanib and SAHA were performed at the same time and share the same control growth curve. Mean ± SEM; *$p < 0.05$ indicates treatment group versus control.

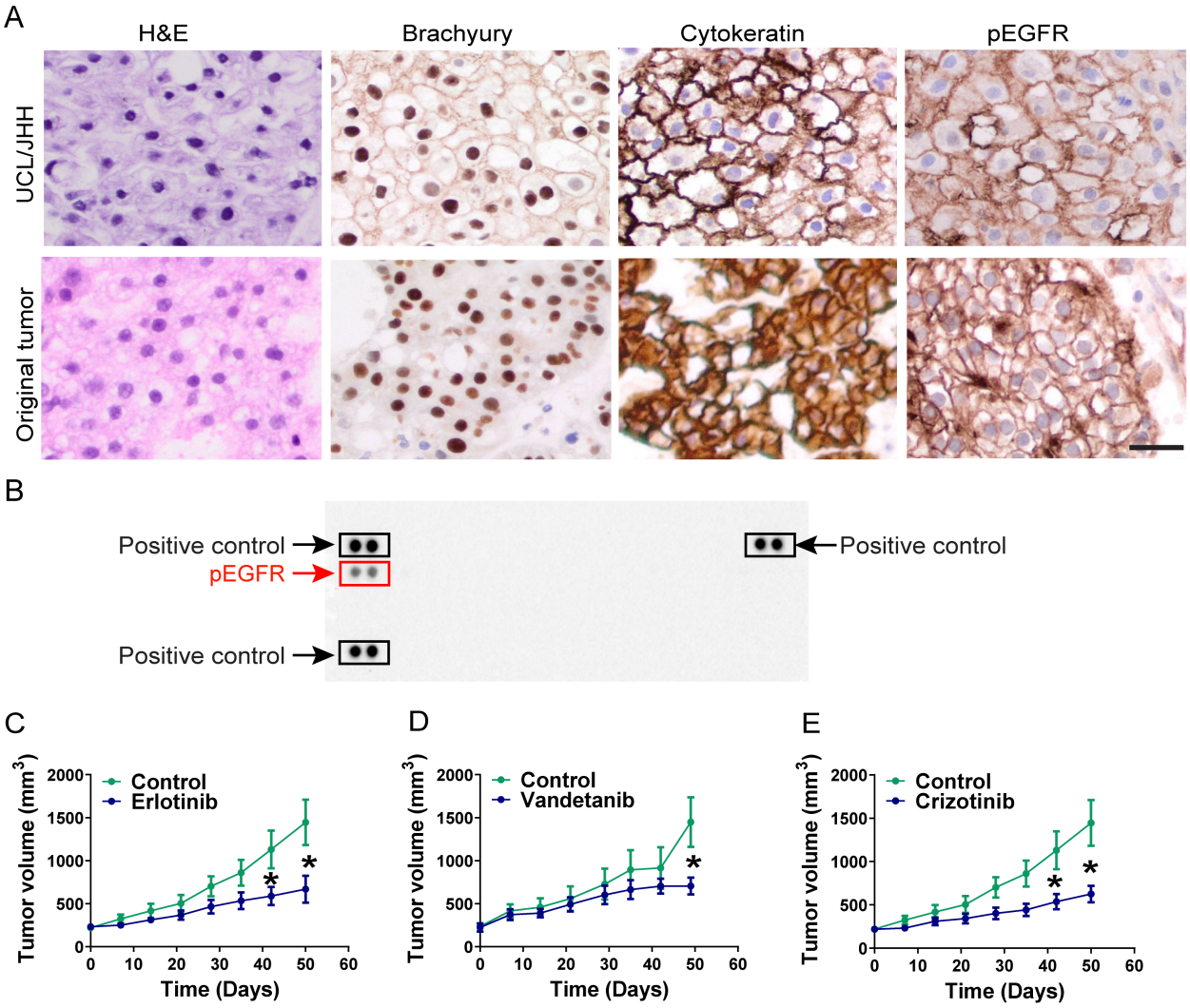

Figure 2. Establishment of a novel chordoma PDX (UCL/JHH) and validation of anti-tumor activity of compounds identified in the initial *in vivo* screen. (A) Representative photomicrographs showing the histological profiles of the UCL/JHH PDX and the original tumor, which were stained with hematoxylin and eosin (H&E) and immunohistochemically with anti-brachyury, anti-pan cytokeratin, and anti-pEGFR antibodies. Scale bar: 100 μm. (B) Receptor tyrosine kinase array revealed activation of EGFR in the PDX UCL/JHH. The presence of activated EGFR (pEGFR) and positive controls are indicated in red and black rectangles, respectively. Athymic nude mice bearing UCL/JHH tumors were treated with erlotinib (C, $n = 6$), vandetanib (D, $n = 5$), and crizotinib (E, $n = 6$), and tumor volumes were measured and plotted. Single treatments of erlotinib and crizotinib were performed in the same experiment and share the same control growth curve. Mean ± SEM; $^*p < 0.05$ indicates treatment group versus control.

Results

BIBX 1382, vandetanib, and crizotinib suppressed chordoma growth *in vivo*

Using our previously characterized chordoma PDX model (JHH-2009-011) [8], the anti-tumor activities of six compounds identified in an NCGC *in vitro* screen with potent anti-chordoma activity [14] were assessed *in vivo*. In addition, inhibitors of c-MET and PDGFR were evaluated as these pathways are expressed and/or activated in chordomas [15–17,30]. The targets, routes of administration, and dosages tested are listed in Table 1. Our data demonstrated that the EGFR inhibitor BIBX 1382, the multi-kinase inhibitor vandetanib, and the c-MET inhibitor crizotinib significantly inhibited chordoma growth *in vivo* (Figure 1A–C, $^*p < 0.05$). By contrast, idarubicin, SAHA, staurosporine, 17-AAG, and imatinib had no significant effects on tumor growth (Figure 1D–H).

Table 2. Genetic comparison of the UCL/JHH PDX and the original chordoma by short tandem repeat profiling.

	Original tumor		UCL/JHH PDX	
Markers	Allele 1	Allele 2	Allele 1	Allele 2
AMEL	X	X	X	X
CSF1PO	12	12	12	12
D13S317	12	12	12	12
D16S539	11	12	11	12
D18S51	18	18	18	18
D21S11	27	30	27	30
D3S1358	16	18	16	16
D5S818	12	12	12	12
D7S820	13	13	12	12
D8S1179	11	16	11	11
FGA	23	23	–	–
Penta D	12	12	12	12
Penta E	15	15	12	15
TH01	9.3	9.3	9.3	9.3
TPOX	8	8	8	8
vWA	14	18	14	18

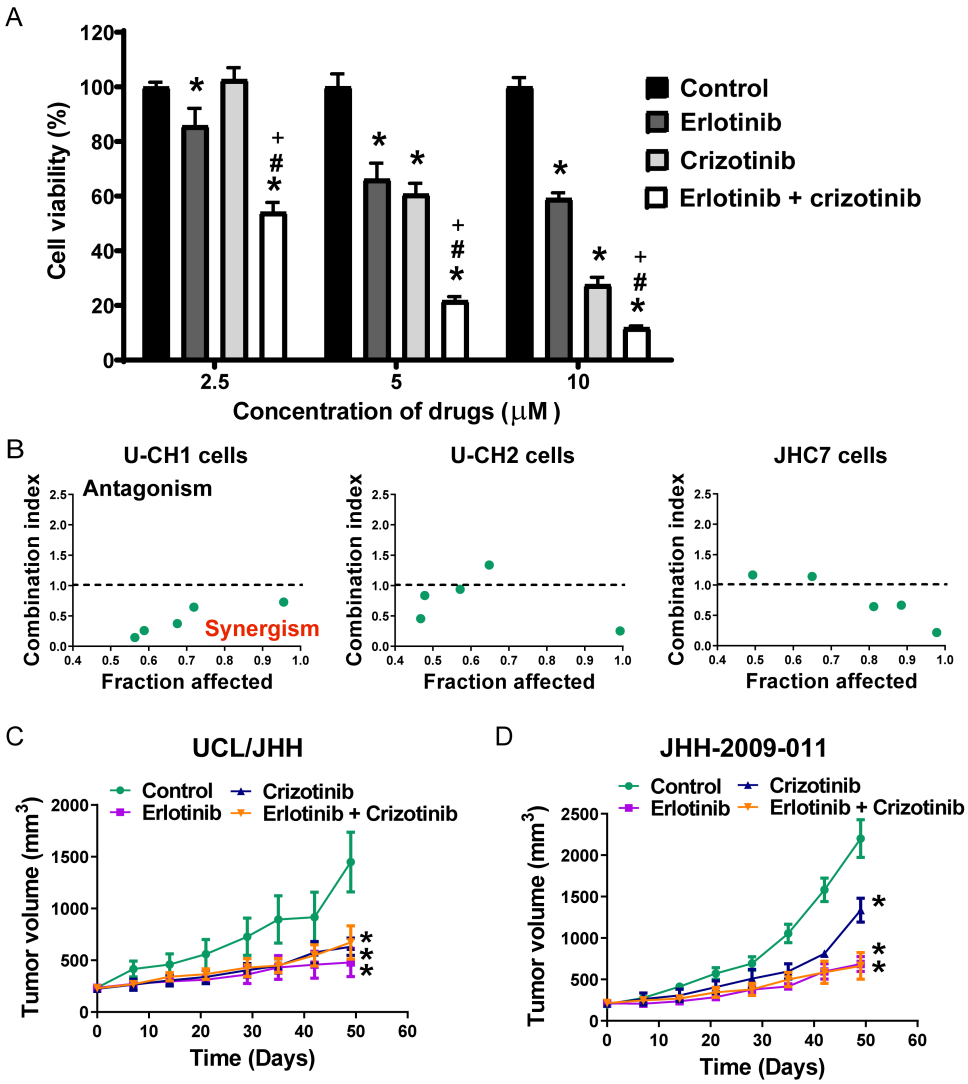

Figure 3. Crizotinib enhances erlotinib activity in chordoma cell lines but not in PDX models. (A) Cell viability was significantly reduced in U-CH1 cells treated with erlotinib and crizotinib at 2.5, 5, and 10 μM, and enhanced activity was seen with co-treatment. Mean ± SEM; $^{*}p < 0.05$ indicates single treatment versus control; $^{+}p < 0.05$ indicates erlotinib versus erlotinib + crizotinib; $^{\#}p < 0.05$ indicates crizotinib versus erlotinib + crizotinib. (B) Combination index analysis of erlotinib and crizotinib in U-CH1, U-CH2, and JHC7 cells. (C, D) Tumor growth of UCL/JHH ($n = 5$) and JHH-2009-011 ($n = 5$ for control and crizotinib groups; $n = 6$ for erlotinib and erlotinib + crizotinib groups) PDXs treated with erlotinib (50 mg/kg per day) or/and crizotinib (25 mg/kg per day) is shown. Mean ± SEM; $^{*}p < 0.05$ indicates treatment group versus control.

Establishment and characterization of a novel chordoma PDX to validate the anti-tumor effect observed in initial *in vivo* screen

To confirm our *in vivo* findings, a novel chordoma PDX (UCL/JHH) was generated from a recurrent sacral tumor in a 51-year-old woman. H&E staining of UCL/JHH PDX and the patient's original tumor showed lobulated tumor cells separated by fibrous septa and physaliphorous cells (Figure 2A). Immunohistochemistry (IHC) for brachyury and cytokeratin showed strong expression in both the UCL/JHH PDX and the original patient's tumor (Figure 2A). Further genomic analysis using short tandem repeat (STR) analysis revealed that UCL/JHH PDX and the original tumor were unique, derived from the same source material, and shared 87% identity (Table 2). Of note, the majority of cells in the UCL/JHH PDX model were positive for phosphorylated EGFR (pEGFR) immunostaining (Figure 2A) and EGFR was the most activated receptor tyrosine kinase on the phospho-receptor tyrosine kinase array (Figure 2B). Taken together, these results show that UCL/JHH PDX retains the genetic and histopathological features of the patient's original tumor. UCL/JHH tumor-bearing animals were treated with erlotinib, vandetanib, and crizotinib. Similar to our findings in JHH-2009-011 (Figure 1B,C) and a previous report [13], all three compounds significantly suppressed tumor growth compared with control mice (Figure 2C–E).

Crizotinib enhanced erlotinib activity *in vitro* but not *in vivo*

Although treatment with compounds that inhibit EGFR resulted in tumor growth inhibition in both animal

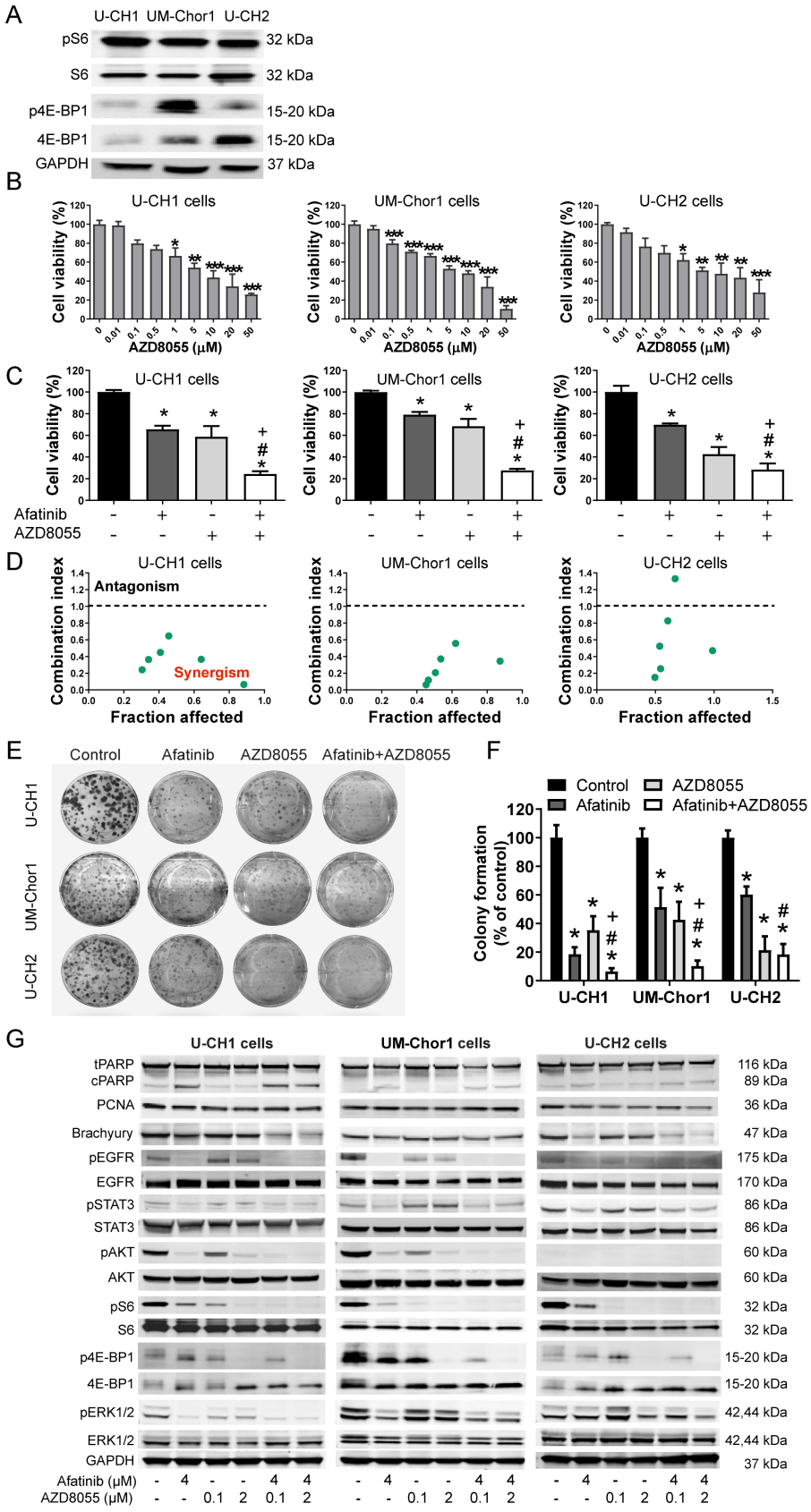

Figure 4 Legend on next page.

models, tumor regression was not observed (Figures 1A, B and 2C,D) [13], which prompted us to evaluate the efficacy of combinatorial therapies. Given that EGFR inhibitors and the c-MET inhibitor crizotinib suppressed chordoma growth *in vivo*, our subsequent analysis focused on co-targeting these two pathways. *In vitro* studies demonstrated that erlotinib alone and crizotinib alone significantly reduced cell viability in U-CH1 cells; notably, co-treatment led to further significant reduction of cell viability compared with treatments with single compounds (Figure 3A) and in a synergistic fashion in this line (Figure 3B).

To elucidate potential mechanisms underlying erlotinib and/or crizotinib-mediated reduced cell viability, drug effects on cell proliferation, cell death, and the expression of brachyury were investigated in three chordoma cell lines (supplementary material, Figure S1A). Co-treatment with erlotinib and crizotinib induced poly(ADP-ribose) polymerase (PARP) cleavage compared with single drug treatments and control in U-CH1, suggesting that co-treatment can induce cell apoptosis in this line. This result was verified by detecting an increased annexin-V-positive cell population using flow cytometry after co-treatment with erlotinib and crizotinib in U-CH1 cells (supplementary material, Figure S1B). No difference in proliferating cell nuclear antigen (PCNA) expression was detected after treatment of erlotinib or/and crizotinib. Aside from a slight decrease in expression of brachyury in U-CH2 cells when treated with crizotinib alone and in combination with erlotinib, brachyury expression was unaffected in the other two cell lines (supplementary material, Figure S1A).

We next evaluated the *in vivo* anti-tumor effect of co-treatment with erlotinib and crizotinib using JHH-2009-011 and UCL/JHH PDXs. While erlotinib and crizotinib significantly inhibited tumor growth as single agents in both models, crizotinib did not enhance erlotinib activity in either model (Figure 3C,D). A slight transient decrease in body weight (10–11%) was observed with combination treatment compared with baseline, which subsequently recovered during the course of therapy (supplementary material, Figure S1C). Tumors from the UCL/JHH *in vivo* experiment were collected at the end of treatment for comparative analyses by western blot with our *in vitro* data. Similar to U-CH1 cells, co-treatment in the PDX increased expression of cleaved PARP compared with single treatments and control (supplementary material, Figure S1A). Based on the lack of combinational activity *in vivo*, we expanded our search and examined other co-targeting strategies.

AZD8055 enhanced afatinib activity *in vitro*

Because activation of the mTOR pathway has been reported in the majority of chordoma patients [31,32], we examined co-targeting this pathway together with EGFR. First, we confirmed that the mTOR pathway was activated *in vitro*, as shown by phosphorylation of S6 and 4E-BP1 in U-CH1, UM-Chor1, and U-CH2 cells (Figure 4A). Treatment with the mTOR inhibitor AZD8055 significantly reduced cell viability in a dose-dependent manner in all three cell lines (Figure 4B). Afatinib, an irreversible EGFR inhibitor, has a unique capacity to inhibit the expression of brachyury compared with other EGFR inhibitors tested (supplementary material, Figure S2); therefore, it was used instead of erlotinib in the subsequent studies. Co-treatment with afatinib and AZD8055 significantly reduced cell viability compared with afatinib or AZD8055 monotherapy (Figure 4C and supplementary material, Figure S3A). Moreover, afatinib and AZD8055 acted synergistically (Figure 4D). We also performed trypan blue and LDH assays, which demonstrated that co-treatment with afatinib and AZD8055 induced more cell death compared with single treatments (supplementary material, Figure S3B,C). Co-treatment with afatinib and AZD8055 also led to inhibition of colony formation, as demonstrated by reducing the number and size of colonies in all three chordoma cell lines (Figure 4E,F). To further evaluate the effect of co-treatment on cell growth, western blot analysis showed increased cell apoptosis, as indicated by the induction of cleaved PARP, which is primarily caused by afatinib treatment in all three cell lines (Figure 4G). Aside from a slight decrease of the expression of PCNA in U-CH1 and U-CH2 cells, PCNA expression was unchanged in UM-Chor1 cells after treatment with the combination. Moreover, co-treatment with afatinib and AZD8055 attenuated the expression of brachyury compared with single agent therapy mainly in U-CH1 cells, and to a lesser extent in U-CH2 cells (Figure 4G), which was confirmed by brachyury immunofluorescence staining (supplementary material, Figure S3D). To determine

Figure 4. AZD8055 enhances the *in vitro* efficacy of afatinib. (A) Representative western blot reveals the expression of pS6, S6, p4E-BP1, and 4E-BP1 in U-CH1, UM-Chor1, and U-CH2 cells. (B) AZD8055 dose-dependently reduced the cell viability of U-CH1, UM-Chor1, and U-CH2 cells. Mean ± SEM; $^{*}p < 0.05$, $^{**}p < 0.01$, $^{***}p < 0.001$ indicate group versus control group. (C) Co-treatment with 2 μM afatinib and 5 μM AZD8055 collectively reduced the cell viability of U-CH1, UM-Chor1, and U-CH2 cells. Mean ± SEM; $^{*}p < 0.05$ indicates group versus control; $^{\#}p < 0.05$ indicates co-treatment versus 2 μM afatinib; $^{+}p < 0.05$ indicates co-treatment versus 5 μM AZD8055. (D) Combination index analysis showing the synergistic effect (CI < 1) of afatinib and AZD8055 in chordoma cells. (E) Representative photomicrographs indicating the colony formation in chordoma cells treated with 0.5 μM afatinib or/and 5 μM AZD8055. (F) The quantification analysis of colony formation following treatment of indicated drugs. Mean ± SEM; $^{*}p < 0.05$ indicates group versus control; $^{\#}p < 0.05$ indicates co-treatment versus afatinib; $^{+}p < 0.05$ indicates co-treatment versus AZD8055. (G) Representative western blot showing the expression of indicated protein in U-CH1, UM-Chor1, and U-CH2 cells treated with afatinib or/and AZD8055.

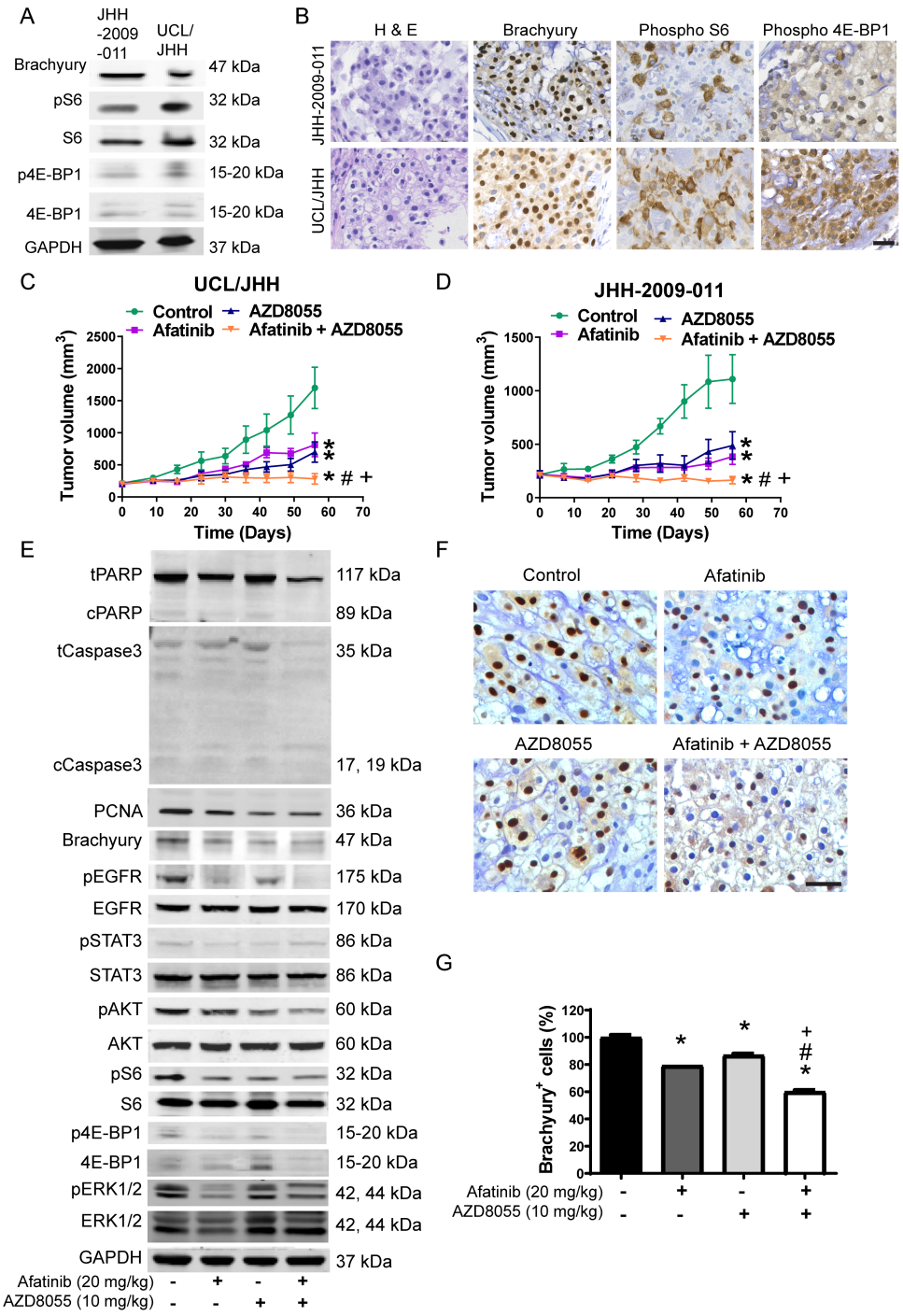

Figure 5. AZD8055 enhances the *in vivo* efficacy of afatinib. Representative western blot (A) and immunohistochemistry (B) showing the expression of brachyury, pS6, S6, p4E-BP1, and 4E-BP1 in JHH-2009-011 and UCL/JHH xenografts. Nude mice bearing (C) PDX UCL/JHH or (D) PDX JHH-2009-011 were treated with afatinib (20 mg/kg per day) and/or AZD8055 (10 mg/kg per day), and the volume of tumor growth was plotted. Mean ± SEM; $n = 5$; $^{*}p < 0.05$ indicates group versus control; $^{\#}p < 0.05$ indicates co-treatment versus afatinib; $^{+}p < 0.05$ indicates co-treatment versus AZD8055. The significant difference with combination treatment in UCL/JHH and JHH-2009-011 started at day 56 and day 49, respectively. (E) Representative western blot reveals the expression of indicated protein in PDX UCL/JHH treated with afatinib or/and AZD8055. (F) Representative immunohistochemical photomicrographs showing expression of brachyury in treated PDX UCL/JHH. Scale bar: 100 μm. (G) The numbers of brachyury-positive cells are quantified. Mean ± SEM; $^{*}p < 0.05$ indicates group versus control; $^{\#}p < 0.05$ indicates co-treatment versus afatinib; $^{+}p < 0.05$ indicates co-treatment versus AZD8055.

the effect of co-treatment on EGFR and mTOR downstream signaling, western blotting showed that co-treatment strongly inhibited the phosphorylation of EGFR, STAT3, AKT, and ERK1/2 compared with controls, which was mainly caused by afatinib treatment, while the decreased phosphorylation of S6 and 4E-BP1 in co-treatment was primarily due to AZD8055 treatment (Figure 4G).

AZD8055 enhanced the *in vivo* efficacy of afatinib in chordoma

We evaluated the anti-tumor effect of co-treatment with afatinib and AZD8055 using chordoma PDX models. Phosphorylation of S6 and 4E-BP1 was detected in untreated PDX models by western blot (Figure 5A) and immunohistochemistry (Figure 5B). In both the JHH-2009-011 and the UCL/JHH chordoma PDX models, afatinib alone, AZD8055 alone, and co-treatment with afatinib and AZD8055 all significantly inhibited tumor growth compared with vehicle-treated controls (Figure 5C,D); combinatorial therapy was well tolerated, with no significant weight loss compared with baseline and no behavioral changes observed (supplementary material, Figure S4A,B). Importantly, co-treatment with afatinib and AZD8055 led to increased tumor growth inhibition (85% inhibition in JHH-2009-011 and 87% inhibition in UCL/JHH), compared with afatinib (65% inhibition in JHH-2009-011 and 55% inhibition in UCL/JHH) or AZD8055 monotherapies (56% inhibition in JHH-2009-011 and 62% inhibition in UCL/JHH). Strikingly, co-treatment was able to completely restrain chordoma growth in both models; no significant differences in tumor size were detected before and after the co-treatment with afatinib and AZD8055 (Figure 5C,D).

We next examined the *in vivo* effects on cell apoptosis and proliferation in the PDX model. Although the cleaved forms of PARP and caspase-3 were not detected in all groups (possibly due to the timing of tumor harvest), the expression of both total PARP and caspase-3 was reduced in the co-treatment group compared with single-treatment groups (Figure 5E). Co-treatment with afatinib and AZD8055 inhibited cell proliferation, as revealed by the reduced PCNA expression compared with control, and this was primarily the result of AZD8055 treatment (Figure 5E). Furthermore, co-treatment attenuated the expression of brachyury (Figure 5E) and significantly reduced the number of brachyury-positive cells compared with control (Figure 5F,G). Afatinib alone inhibited phosphorylation of EGFR and AZD8055 alone inhibited phosphorylation of S6 and 4E-BP1, showing on-target activity of both drugs *in vivo*. Interestingly, the co-treatment with afatinib and AZD8055 collectively suppressed the activation of EGFR and AKT compared with single treatments (Figure 5E).

Discussion

Given the poor clinical outcome for patients with chordoma, extensive efforts have been undertaken to develop therapies against chordoma. An NCGC Pharmaceutical Collection (NPC) screen containing approximately 2800 clinically approved and investigational drugs was performed in chordoma cell lines, identifying numerous drugs that inhibited chordoma growth *in vitro* [14]. In the current study, we evaluated the *in vivo* anti-tumor activity of potent agents including BIBX 1382, vandetanib, idarubicin, SAHA, staurosporine, and 17-AAG identified in the NCGC screen as well as inhibitors of c-MET and PDGFR. Using our initial chordoma PDX model JHH-2009-011 [8], we demonstrated that BIBX 1382, vandetanib, and crizotinib inhibited tumor growth. To evaluate this finding in another *in vivo* model, a second chordoma PDX (UCL/JHH) was established and validated. STR profiling revealed that the UCL/JHH PDX model and its parental tumor samples were unique and derived from the same source material, as they showed over 80% match required for STR profiling criteria in ATCC guidelines. A few differences in some of the markers were identified and could be explained by the heterogeneity of the original tumor material and/or by minor genetic drift events during xenograft expansion. Using this second model, we found tumor growth inhibition in tumor-bearing animals treated with erlotinib, vandetanib, or crizotinib.

EGFR is activated in chordoma and previous studies by our group and others, together with our current study, have shown that EGFR inhibitors suppress the growth of chordoma cell lines and/or PDX models [13,25,33], suggesting that targeting the EGFR pathway is a potentially effective therapeutic strategy for patients with chordoma. In clinical studies, EGFR inhibitor monotherapy has resulted in partial regression and/or clinical improvement in patients with chordoma [34–37]. Of the EGFR inhibitors, the second-generation EGFR inhibitor afatinib is the most promising chordoma therapeutic agent, not only because it is an irreversible EGFR inhibitor [38] but also because it reduces the expression of brachyury [25], a gene critical for chordoma development [2–4], making afatinib unique compared with other EGFR inhibitors such as erlotinib, vandetanib, and BIBX 1382. We were also interested in identifying agents that would enhance the effects of EGFR inhibition in our models. Clinically, there is already a move towards combined treatments with some favorable indicators: the combination of erlotinib and insulin-like growth factor receptor (IGF1R) inhibitor linsitinib [37,39] and a combination of erlotinib and the VEGF inhibitor bevacizumab [40] have exhibited partial clinical improvement in patients with chordomas, making the case that combined therapies can be tolerated.

In addition to EGFR inhibitors, we demonstrated that the c-MET inhibitor crizotinib significantly reduced cell viability in chordoma cell lines and inhibited tumor growth in PDX models. It has been previously reported that the combination of the EGFR inhibitor sapitinib and the c-MET inhibitor crizotinib synergistically reduced cell viability in U-CH2 [33]. We found that the combination of erlotinib with crizotinib exhibited a synergistic effect in U-CH1 *in vitro*; however, the combination of erlotinib and crizotinib did not result in greater inhibition of tumor growth *in vivo* compared with erlotinib alone. Due to the lack of enhanced activity *in vivo* and the reduction of brachyury seen with afatinib, we expanded our search for other agents to combine with afatinib.

There is increasing evidence that the mTOR pathway is important in chordoma [31,41,42], and the classic mTOR inhibitor rapamycin has been shown to suppress

the survival and proliferation of chordoma cells, leading to a substantial reduction of tumor growth in animal models and in patients [43]. Unlike rapamycin, which is a potent inhibitor of mTORC1 but less sensitive to mTORC2 [44], AZD8055 is a dual mTORC1/2 inhibitor that exhibits anti-tumor activity in a variety of tumors [26,45]. In addition, AZD8055 decreases the expression of mTORC2 substrates such as phosphorylated AKT [26,46], a protein kinase widely activated in the majority of chordomas [31,47], while rapamycin mainly inhibits mTORC1 activation, leading to hyperactivation of AKT [46].

In this study, we have shown that the combination of afatinib and AZD8055 synergistically reduced the cell viability of chordoma cell lines; furthermore, co-administration of afatinib and AZD8055 completely arrested the growth of chordoma PDXs. Our data presented here support the evaluation of this combination in patients with chordoma.

Acknowledgements

The U-CH1 and U-CH2 cell lines were kindly provided by the Chordoma Foundation; the JHC7 cell line was kindly provided by Alfredo Quiñones-Hinojosa; and idarubicin, SAHA, staurosporine, and 17-AAG were kindly provided by NCATS. We would like to thank Josh Sommer and the Chordoma Foundation for their support and assistance. We thank past and present members of the Skull Base and Hunterian Neurosurgical Research Laboratories. We are grateful to our patients for their courage and generosity and thank the biobank team for consenting patients and accessing samples. This study was supported by the Chordoma Foundation, Johns Hopkins University School of Medicine Department of Neurosurgery, and Michael and Noreen Potempa (to GLG) and Chordoma UK, the Skeletal Cancer Trust, the Royal National Orthopaedic Hospital NHS Trust R&D Programme, the National Institute for Health Research UCLH Biomedical Research Centre, and the UCL Experimental Cancer Centre (to AMF). This work was also supported in part by the Intramural Research Program of the NCATS, NIH (to MX). LC was funded by the Chordoma Foundation. CLH is supported by NIH grant 1U01CA231776.

Author contributions statement

GLG, CLH, TZ and IS conceived and designed the project. TZ, IS, TW, HZ, CJ, NC, JR and LC carried out experiments and analyzed data. MX provided experimental materials. PCB, AMF and GLG acquired patient samples and provided clinical expertise. TZ, IS, CLH, AMF and GLG wrote, reviewed, and revised the manuscript. All the authors reviewed and approved the final version of the manuscript.

References

1. McMaster ML, Goldstein AM, Bromley CM, *et al*. Chordoma: incidence and survival patterns in the United States, 1973–1995. *Cancer Causes Control* 2001; **12:** 1–11.
2. Nibu Y, José-Edwards DS, Di Gregorio A. From notochord formation to hereditary chordoma: the many roles of *Brachyury*. *Biomed Res Int* 2013; **2013:** 826435.
3. Yang XR, Ng D, Alcorta DA, *et al*. *T* (brachyury) gene duplication confers major susceptibility to familial chordoma. *Nat Genet* 2009; **41:** 1176–1178.
4. Presneau N, Shalaby A, Ye H, *et al*. Role of the transcription factor *T* (brachyury) in the pathogenesis of sporadic chordoma: a genetic and functional-based study. *J Pathol* 2011; **223:** 327–335.
5. Walcott BP, Nahed BV, Mohyeldin A, *et al*. Chordoma: current concepts, management, and future directions. *Lancet Oncol* 2012; **13:** e69–e76.
6. Stacchiotti S, Sommer J, Chordoma Global Consensus Group. Building a global consensus approach to chordoma: a position paper from the medical and patient community. *Lancet Oncol* 2015; **16:** e71–e83.
7. Chambers KJ, Lin DT, Meier J, *et al*. Incidence and survival patterns of cranial chordoma in the United States. *Laryngoscope* 2014; **124:** 1097–1102.
8. Siu IM, Salmasi V, Orr BA, *et al*. Establishment and characterization of a primary human chordoma xenograft model. *J Neurosurg* 2012; **116:** 801–809.
9. Dewaele B, Maggiani F, Floris G, *et al*. Frequent activation of EGFR in advanced chordomas. *Clin Sarcoma Res* 2011; **1:** 4.
10. Shalaby A, Presneau N, Ye H, *et al*. The role of epidermal growth factor receptor in chordoma pathogenesis: a potential therapeutic target. *J Pathol* 2011; **223:** 336–346.
11. Tamborini E, Virdis E, Negri T, *et al*. Analysis of receptor tyrosine kinases (RTKs) and downstream pathways in chordomas. *Neuro Oncol* 2010; **12:** 776–789.
12. Fasig JH, Dupont WD, LaFleur BJ, *et al*. Immunohistochemical analysis of receptor tyrosine kinase signal transduction activity in chordoma. *Neuropathol Appl Neurobiol* 2008; **34:** 95–104.
13. Siu IM, Ruzevick J, Zhao Q, *et al*. Erlotinib inhibits growth of a patient-derived chordoma xenograft. *PLoS One* 2013; **8:** e78895.
14. Xia M, Huang R, Sakamuru S, *et al*. Identification of repurposed small molecule drugs for chordoma therapy. *Cancer Biol Ther* 2013; **14:** 638–647.
15. Tosuner Z, Bozkurt SU, Kiliç T, *et al*. The role of EGFR, hepatocyte growth factor receptor (c-Met), c-ErbB2 (HER2-neu) and clinicopathological parameters in the pathogenesis and prognosis of chordoma. *Turk Patoloji Derg* 2017; **33:** 112–120.
16. Akhavan-Sigari R, Gaab MR, Rohde V, *et al*. Expression of PDGFR-α, EGFR and c-MET in spinal chordoma: a series of 52 patients. *Anticancer Res* 2014; **34:** 623–630.
17. Akhavan-Sigari R, Abili M, Gaab MR, *et al*. Immunohistochemical expression of receptor tyrosine kinase PDGFR-α, c-Met, and EGFR in skull base chordoma. *Neurosurg Rev* 2015; **38:** 89–98; discussion 98–99.
18. Stacchiotti S, Longhi A, Ferraresi V, *et al*. Phase II study of imatinib in advanced chordoma. *J Clin Oncol* 2012; **30:** 914–920.
19. Gule MK, Chen Y, Sano D, *et al*. Targeted therapy of VEGFR2 and EGFR significantly inhibits growth of anaplastic thyroid cancer in an orthotopic murine model. *Clin Cancer Res* 2011; **17:** 2281–2291.
20. Tanizaki J, Okamoto I, Okamoto K, *et al*. MET tyrosine kinase inhibitor crizotinib (PF-02341066) shows differential antitumor effects in non-small cell lung cancer according to *MET* alterations. *J Thorac Oncol* 2011; **6:** 1624–1631.
21. Thiemann M, Oertel S, Ehemann V, *et al*. *In vivo* efficacy of the histone deacetylase inhibitor suberoylanilide hydroxamic acid in combination with radiotherapy in a malignant rhabdoid tumor mouse model. *Radiat Oncol* 2012; **7:** 52.

22. Kumar S, Tomar MS, Acharya A. Chelerythrine delayed tumor growth and increased survival duration of Dalton's lymphoma bearing BALB/c H^{2d} mice by activation of NK cells *in vivo*. *J Cancer Res Ther* 2015; **11:** 904–910.
23. Waza M, Adachi H, Katsuno M, *et al*. 17-AAG, an Hsp90 inhibitor, ameliorates polyglutamine-mediated motor neuron degeneration. *Nat Med* 2005; **11:** 1088–1095.
24. Beppu K, Jaboine J, Merchant MS, *et al*. Effect of imatinib mesylate on neuroblastoma tumorigenesis and vascular endothelial growth factor expression. *J Natl Cancer Inst* 2004; **96:** 46–55.
25. Magnaghi P, Salom B, Cozzi L, *et al*. Afatinib is a new therapeutic approach in chordoma with a unique ability to target EGFR and brachyury. *Mol Cancer Ther* 2018; **17:** 603–613.
26. Chresta CM, Davies BR, Hickson I, *et al*. AZD8055 is a potent, selective, and orally bioavailable ATP-competitive mammalian target of rapamycin kinase inhibitor with *in vitro* and *in vivo* antitumor activity. *Cancer Res* 2010; **70:** 288–298.
27. Chen X, Guan Z, Lu J, *et al*. Synergistic antitumor effects of cMet inhibitor in combination with anti-VEGF in colorectal cancer patient-derived xenograft models. *J Cancer* 2018; **9:** 1207–1217.
28. Hsu W, Mohyeldin A, Shah SR, *et al*. Generation of chordoma cell line JHC7 and the identification of Brachyury as a novel molecular target. *J Neurosurg* 2011; **115:** 760–769.
29. Chou TC. Theoretical basis, experimental design, and computerized simulation of synergism and antagonism in drug combination studies. *Pharmacol Rev* 2006; **58:** 621–681.
30. Tamborini E, Miselli F, Negri T, *et al*. Molecular and biochemical analyses of platelet-derived growth factor receptor (PDGFR) B, PDGFRA, and KIT receptors in chordomas. *Clin Cancer Res* 2006; **12:** 6920–6928.
31. Presneau N, Shalaby A, Idowu B, *et al*. Potential therapeutic targets for chordoma: PI3K/AKT/TSC1/TSC2/mTOR pathway. *Br J Cancer* 2009; **100:** 1406–1414.
32. Tauziéde-Espariat A, Bresson D, Polivka M, *et al*. Prognostic and therapeutic markers in chordomas: a study of 287 tumors. *J Neuropathol Exp Neurol* 2016; **75:** 111–120.
33. Scheipl S, Barnard M, Cottone L, *et al*. EGFR inhibitors identified as a potential treatment for chordoma in a focused compound screen. *J Pathol* 2016; **239:** 320–334.
34. Launay SG, Chetaille B, Medina F, *et al*. Efficacy of epidermal growth factor receptor targeting in advanced chordoma: case report and literature review. *BMC Cancer* 2011; **11:** 423.
35. Houessinon A, Boone M, Constans JM, *et al*. Sustained response of a clivus chordoma to erlotinib after imatinib failure. *Case Rep Oncol* 2015; **8:** 25–29.
36. Lindén O, Stenberg L, Kjellén E. Regression of cervical spinal cord compression in a patient with chordoma following treatment with cetuximab and gefitinib. *Acta Oncol* 2009; **48:** 158–159.
37. Macaulay VM, Middleton MR, Eckhardt SG, *et al*. Phase I dose-escalation study of linsitinib (OSI-906) and erlotinib in patients with advanced solid tumors. *Clin Cancer Res* 2016; **22:** 2897–2907.
38. Solca F, Dahl G, Zoephel A, *et al*. Target binding properties and cellular activity of afatinib (BIBW 2992), an irreversible ErbB family blocker. *J Pharmacol Exp Ther* 2012; **343:** 342–350.
39. Aleksic T, Browning L, Woodward M, *et al*. Durable response of spinal chordoma to combined inhibition of IGF-1R and EGFR. *Front Oncol* 2016; **6:** 98.
40. Asklund T, Sandström M, Shahidi S, *et al*. Durable stabilization of three chordoma cases by bevacizumab and erlotinib. *Acta Oncol* 2014; **53:** 980–984.
41. Schwab J, Antonescu C, Boland P, *et al*. Combination of PI3K/mTOR inhibition demonstrates efficacy in human chordoma. *Anticancer Res* 2009; **29:** 1867–1871.
42. Chen K, Mo J, Zhou M, *et al*. Expression of PTEN and mTOR in sacral chordoma and association with poor prognosis. *Med Oncol* 2014; **31:** 886.
43. Ricci-Vitiani L, Runci D, D'Alessandris QG, *et al*. Chemotherapy of skull base chordoma tailored on responsiveness of patient-derived tumor cells to rapamycin. *Neoplasia* 2013; **15:** 773–782.
44. Kennedy BK, Lamming DW. The mechanistic target of rapamycin: the Grand ConducTOR of metabolism and aging. *Cell Metab* 2016; **23:** 990–1003.
45. Chen Y, Lee CH, Tseng BY, et al. AZD8055 exerts antitumor effects on colon cancer cells by inhibiting mTOR and cell-cycle progression. *Anticancer Res* 2018; **38**: 1445–1454.
46. Marshall G, Howard Z, Dry J, *et al*. Benefits of mTOR kinase targeting in oncology: pre-clinical evidence with AZD8055. *Biochem Soc Trans* 2011; **39:** 456–459.
47. de Castro CV, Guimaraes G, Aguiar S Jr, *et al*. Tyrosine kinase receptor expression in chordomas: phosphorylated AKT correlates inversely with outcome. *Hum Pathol* 2013; **44:** 1747–1755.

SUPPLEMENTARY MATERIAL ONLINE

Figure S1. Co-treatment with erlotinib and crizotinib *in vitro* and *in vivo*

Figure S2. The expression of pEGFR, EGFR, and brachyury in U-CH1 cells treated with single EGFR inhibitors

Figure S3. Cell viability, cytotoxicity, and expression of brachyury in chordoma cells treated with afatinib alone, AZD8055 alone, or in combination

Figure S4. Body weights of PDX mice

Table S1. Antibodies used in this study

Table S2. STR analysis of chordoma cell lines

Appendix S1. Original images of western blots used in this article